Prediction of Tonal Aerodynamic Noise from Open Rotors

Anupam Sharma* and Hsuan-nien Chen†

Aerodynamics & Aeroacoustics Laboratory - Niskayuna,

Aero, Thermal, and Mechanical Systems,

General Electric Global Research Center, One Research Circle, Niskayuna, NY, 12309, USA

A numerical approach for predicting tonal aerodynamic noise from "open rotors" is presented. "Open rotor" refers to an engine architecture with a pair of counter-rotating propellers. Typical noise spectra from an open rotor consist of dominant tones, which arise due both to steady loading/thickness, and due to aerodynamic interaction between the two bladerows. The proposed prediction approach utilizes Reynolds Averaged Navier Stokes (RANS) Computational Fluid Dynamics (CFD) simulations to obtain near-field description of the noise sources. The near-to-far-field propagation is then carried out by solving the Ffowcs Williams-Hawkings equation. Since the interest of this paper is limited to tone noise, a linearized, frequency domain approach is adopted to solve the wake/vortex-blade interaction problem.

This paper focuses primarily on the speed scaling of the aerodynamic tonal noise from open rotors. Even though there is no theoretical mode cut-off due to the absence of the duct in open rotors, the far-field noise is a strong function of the azimuthal mode order. While the former has circumferential modes of high order, due to the relatively large number of blades ($\approx 10 - 12$), the latter typically has modes of small orders. The high mode orders have very low radiation efficiency and exhibit very strong scaling with Mach number, while the low mode orders show a relatively weaker scaling. The prediction approach is able to capture the speed scaling (observed in experiment) of the overall aerodynamic noise very well.

I. Introduction

SINGLE rotation propellers are highly efficient but are restricted to low forward flight speeds and are also limited in the thrust they can generate. A counter-rotating propeller design provides higher thrust and high aerodynamic efficiency at high flight speeds. This is possible because the aft, counter-rotating bladerow takes out the swirl put in by the front rotor. The fuel burn benefit over conventional, ducted fan designs is estimated to be more than 10 percent. A counter-rotating pusher propeller configuration is considered in this report and will henceforth be referred to as "open rotor" (see Fig. 1).

One of the technology roadblocks for the open rotor architecture is the associated aerodynamic noise. The noise spectra from an open rotor appear overwhelmingly tonal however the broadband noise contributes significantly to the overall EPNL (effective perceived noise levels).[1] The tonal noise is caused by the two sets of rotors, the aerodynamic and aeroacoustic interaction between the rotors, and the interaction between the rotors and the pylon/wing/fuselage; the same interaction also produces broadband noise when the interaction involves flow turbulence.

A methodology for numerical prediction of open rotor aerodynamic tone noise is presented here. The approach employs three-dimensional, RANS (for steady loading and thickness noise) and time-linearized RANS (for interaction noise) simulations to characterize noise sources in the near field. Such an approach has previously been successfully used to predict tone noise from fan-OGV interaction in a ducted configuration.[2,3,4] For an open rotor, an additional step of near-to-far field radiation is required, which is carried

*Now Assistant Professor at Iowa State University, sharma@iastate.edu, AIAA Senior Member

†Mechanical Engineer, K1 2C-35, chen@ge.com, AIAA Member

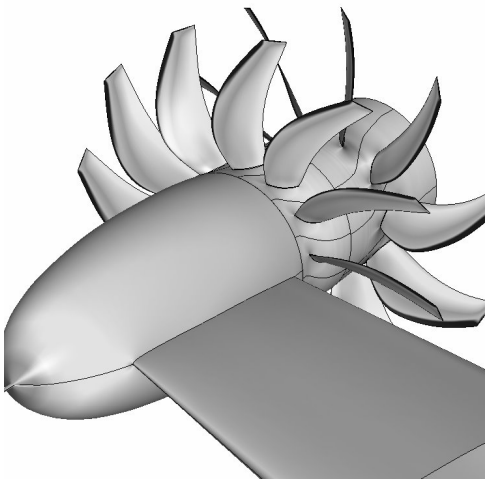

Figure 1. Open rotor configuration considered here for noise assessment.

out by solving the Ffowcs Williams-Hawkings (FW-H) equation[5] using the near-field sources defined on a translating permeable surface. General Electric Company's proprietary flow solver, TACOMA[2,6,7] is used to carry out all flow solutions. A separate, frequency domain, FW-H solver has been developed which has been validated (results in following sections) against analytical solutions of canonical problems.

The concept of counter-rotating propellers has been around for some time and hence there is a rich history of publications in the area of noise from such devices. Hubbard[8] was the first to lay the foundations of counter-rotation propeller noise theory, which Hanson[9,10] elaborated on and developed formulae for analytically predicting noise due to aerodynamic interference (wake interaction) between the two bladerows of a counter-rotating propeller. Hanson[9] also investigated the phenomenon of acoustic interference between the two rotors and between multiple modes from the same rotor. Several efforts have been devoted also into investigating the effects of angle of attack and a substantial increase in noise is observed when these machines are operated in non-uniform flow, see e.g., Mani[11] and Hanson.[12]

Among recent efforts, Carazo *et al.* [13] demonstrated an analytical method for predicting tonal noise from open rotors, wherein the unsteady loading on the aft bladerow due to wake interaction is computed using Amiet's theory. Noise due only to dipole sources was considered and a far-field radiation model was derived from the formulation of a rotating acoustic dipole embedded in a uniform meanflow. Blandeau and Joseph[14] have further demonstrated an analytical capability to predict broadband noise in open rotors due to wake interaction between bladerows. The turbulence is assumed to be homogeneous and isotropic in their analyses.

In contrast to the methods based on classical acoustics (mentioned above), some effort has gone into using a 3-D, Unsteady Reynolds Averaged Navier Stokes (U-RANS) approach for noise prediction, see e.g., Peters and Spakovszky.[15] While theoretically, such a direct simulation approach should resolve all necessary physics of noise generation mechanisms, it faces the challenge of simultaneously resolving both the meanflow hydrodynamic scales and the small acoustic amplitudes. The linearized RANS approach utilized in the current paper isolates the acoustic problem by linearizing about the meanflow and hence permits accurate resolution of acoustics.

Parry *et al.* [1] investigated the relative importance of tonal versus broadband noise from "isolated" open rotors at zero angle of attack (similar configuration as considered here) and concluded that although there are a plethora of tones with significant protrusion above broadband noise, on a one-third octave level, the broadband noise cannot be ignored. While it is evidently important, no attempt is made here to predict broadband noise. In later sections, comparisons are drawn between measurements and prediction; the test data is decomposed into tonal and broadband components in a manner similar to that described in reference.[1]

Shielding of aerodynamic noise is one way to mitigate the noise challenge posed by the open rotor architecture. Towards this, Stephens and Envia[16] reported the experimental findings of an acoustic shielding experiment carried out in the 9" x 15" low-speed wind tunnel (LSWT) at NASA Glenn. They tested acoustic shielding from two (long and short) plates that are representative of an airplane wing or a horizontal/vertical stabilizer. They[16] also mention that the spatial resolution of the microphones is not enough to accurately

resolve tonal noise directivity, as it can be very peaky.

The following section describes the prediction process followed by validation against analytical solutions and comparisons against experimental data.

II. Prediction Process

The proposed open rotor aerodynamic noise prediction process involves multiple steps, which are summarized below. A flowchart illustrating the process flow is also provided in Fig. 2.

1. Multi-stage, RANS calculations are performed using TACOMA[6,7] to compute meanflow solutions. One passage of each bladerow is simulated with periodic boundary conditions across passage boundaries (see Fig. 3). For each rotor, the simulation is performed in its frame of reference enabling steady state simulation for meanflow calculation. For validation cases, where measured aerodynamic performance data is available, the blade pitch is iteratively changed in CFD until shaft horse power (SHP) between the CFD and data are matched. The choice of matching the shaft power as opposed to thrust, and the use of blade pitch as opposed to blade speed to match SHP (or thrust) is arbitrary. Changing the blade speed certainly changes the frequencies, however whether this is more significant in comparison to change in noise levels due to mean loading change (due to blade pitch adjustment) is debatable.

2. Rotor alone noise sources (that due to blade thickness and steady loading) are obtained directly from the RANS simulations of step 1. Primitive flow variables are extracted on surfaces if front of, above, and aft of the simulated blade, which are then replicated (as many times as the number of blades) to form a full annulus surface enclosing all the blades of a rotor (see Fig. 4). This is the FW-H surface over which the boundary integral is performed for far-field noise prediction. Such a surface is also referred to as "permeable" surface as it allows flow through it. One of the benefits of using such a surface is that it only translates with the engine hence making the FW-H surface solver simpler; a surface on or around the individual blades (that rotates with the blades) will accelerate because of rotation. The time history for rotor alone (steady field) is obtained simply by rotating the flow variables on the FW-H surface with the shaft rotation rate. This is achieved cheaply by using uniform grid distribution in the circumferential direction and using the *CSHIFT* routine in Fortran 90.

3. For rotor-rotor interaction noise, an additional RANS solution is carried out in the gap region between the two bladerows. This is performed on a wake-tracking grid, to allow better resolution of the velocity gradients in the wake and hence minimize numerical errors. This procedure has previously been demonstrated by the authors[17] for ducted fans. From this solution, the wake is extracted and decomposed into the front rotor blade passing frequency harmonics. Frequency domain, linearized unsteady Navier-Stokes analyses are then carried out independently for each harmonic. Only a single passage of the aft bladerow has to be simulated by applying the phase lag condition on the domain boundaries in the circumferential direction. Each rotor wake harmonic scatters into multiple frequencies (frequency scattering) as it interacts with the spinning aft rotor and produces what are often referred to as "sum" and "difference" tones. The unsteady primitive variables are extracted from the single-passage unsteady calculation and processed (using the phase lag boundary condition) to generate data on the full-annulus FW-H surface. The FW-H solver uses time-accurate primitive flow variables on the permeable surface as input. The frequency domain solution is thus converted to time domain by performing an inverse Fourier transform.

4. The last step involves FW-H equation solution using the time-dependent flow information on the FW-H surface. This step is the same for rotor alone and interaction noise prediction. Radiated sound power level can be obtained by integrating the sound intensity flux through a sphere surrounding the open rotor (sound source). The microphones in the experiments used for validation are on a sideline (parallel to the engine centerline) arc (see Fig. 5). Sound intensity flux through the cylindrical surface formed by the revolving the arc by 360^0 is therefore used as the sound power metric to compare predictions to measurements. Axi-symmetric sound field is therefore assumed, which holds true when each tone has only one azimuthal (circumferential) mode. When multiple azimuthal modes are present, constructive and destructive interference in the azimuthal direction determines the azimuthal directivity. This assumption however should be true for most of the tones in consideration here assuming that the model is at perfectly zero angle of attack. One of the tones for a 12x10 configuration, for example,

that will have multiple azimuthal modes is the tone at frequency 70Ω (Ω being the shaft rotation rate) as it arises from the combination (sum) of 5^{th} harmonic of the front rotor with the 1^{st} harmonic of the aft rotor ($(5 \times 12 + 1 \times 10)\Omega$) as well as the 7^{th} harmonic ($7 \times 10\Omega$) of the aft rotor.

Furthermore, the sound power radiated at very shallow angles, not covered by the microphones in the experiments, is ignored in the comparisons.

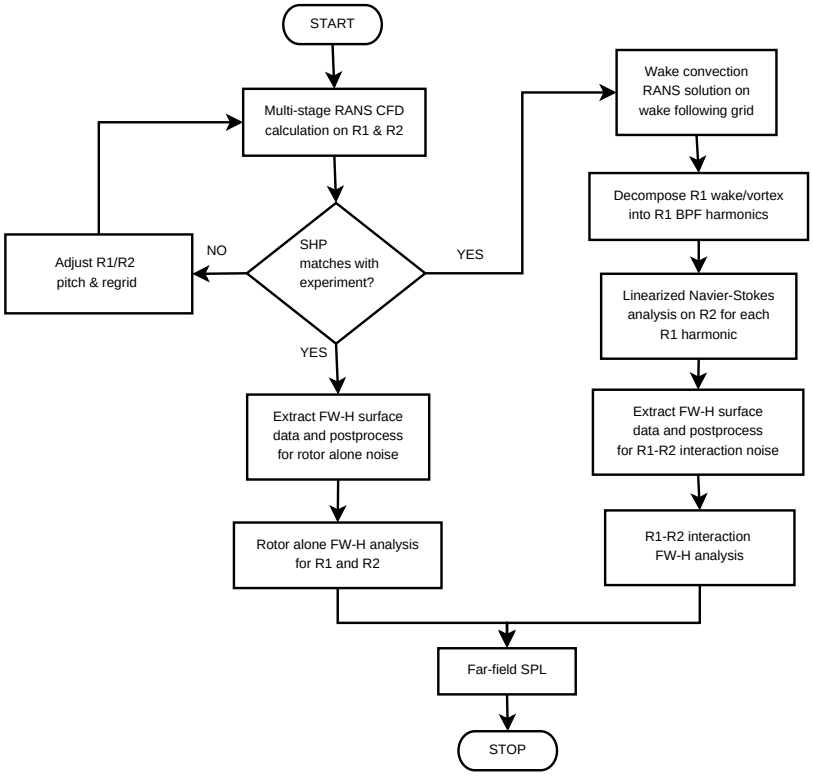

Figure 2. Flowchart of the open rotor noise prediction process.

III. Results

Results from a recent test conducted at the NASA 9'x15' low speed wind tunnel (LSWT) are used to verify the accuracy of the proposed prediction process. One of the many configurations tested in this campaign was the so-named F31A31 historical baseline design. This geometry has a 12-bladed front rotor and a 10-bladed aft rotor. Around the speed/thrust of interest, the interaction tones dominate over the rotor-alone tones (arising from steady thickness and loading noise) and hence comparison of interaction tones between data and predictions is the focus here.

A. Ffowcs Williams-Hawkings Equation Solver

The Ffowcs Williams-Hawkings (FW-H) equation is a re-formulation of the linearized Euler equations using Lighthill's acoustic analogy. A frequency domain formulation of the FW-H equation is used here and the equations are provided in Appendix A.

A frequency domain FW-H equation solver is developed and validated against analytical solutions for point sources (monopole, dipole, and quadrupole) in a quiescent medium. A cube is defined around the point source at which the complete flow-field (density, pressure, and velocities) due to the source are computed analytically. The information on the six faces of the cube is then used by the FW-H solver to compute the sound pressure outside of the cube. Far-field directivities are compared for the three sources in Fig. 6, where an excellent agreement can be observed.

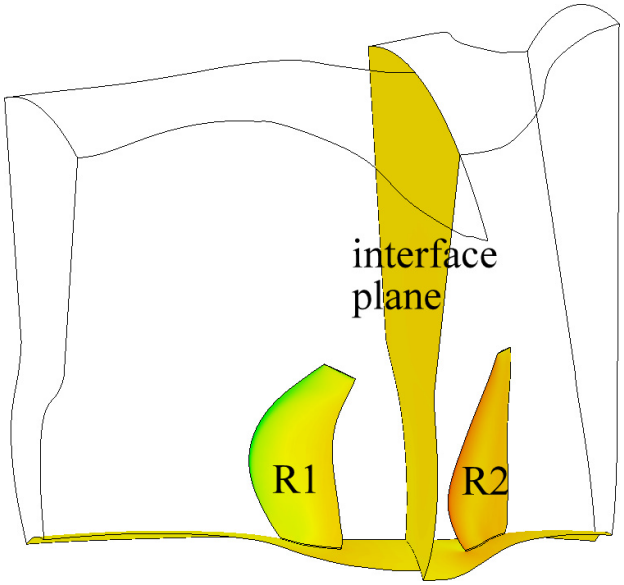

Figure 3. Multi-stage analysis configuration showing one blade each of the two bladerows of the F31A31 design and the interface plane. The front bladerow is referred to as R_1 and the aft, R_2.

Predictions are also made in the near field of the source, although it should be borne in mind that the derivation of the FW-H equation itself makes the approximation that the observer is in the far field. Hence the near-field solution cannot be expected to be exact. Comparisons are nevertheless made (see Fig. 7) in the near field as well, and are found to be reasonable except very near the surface. In Fig. 7, the nearest surface point is located at 2.12 (shown by the arrow in the figure). The near field of dipole and quadrupole sources is reasonably well captured, while the far-field prediction is excellent.

Since the interest is in predicting open rotor noise in flight condition (non-zero forward velocity), the FW-H code is also verified against analytical solution of a point source in a moving medium. Three different flight speeds are considered, namely Mach number equal to 0.25, 0.5, and 0.75. This adequately covers the range of flight speeds of interest although the focus of this paper is on noise during take-off, when the flight Mach number is around 0.25. Directivity comparisons in the far-field showing excellent agreement are plotted in Fig. 8.

The above validation cases provide sufficient confidence in the accuracy of the FW-H solver to attempt the open rotor noise prediction.

B. Validation Against Test Data

For comparison against test data, we focus our attention on the F31A31 geometry, a 12×10 configuration. The present investigation is further limited to investigating the variation of noise with blade tip speed (RPM), while keeping the blade stagger angle fixed - the engine thrust is therefore not held constant. A number of changes occur with speed that all attribute to noise increase with speed in an open rotor. Among these are - (1) increase in radiation efficiency of the mode, (2) increase in wake deficit (due to increased front rotor incidence), and (3) increased unsteady lift on the aft rotor due to (a) high relative velocity, and (b) high mean loading (quadrupole source). The scaling with Mach number of different tones is determined by which of these dominate.

It is observed that the proposed procedure for open rotor noise prediction does remarkably well in predicting the speed scaling of the rotor-rotor interaction tones, as can be seen in Figs. 9 and 10, even though the absolute noise levels are slightly over-predicted. The following nomenclature is used to represent the tones: $[a, b]$ refers to the tone at frequency $a\times$R1 BPF + $b\times$R2 BPF. In the cases considered here, both rotors (R1 and R2) rotate at same shaft rotation rate, Ω. The sum tone $[a, b]$ therefore has a frequency of $(a\times\text{N1} + b\times\text{N2})\Omega$, where N1 and N2 are R1 and R2 blade counts respectively. Appendix B provides a mathematical reasoning for why the "sum" and "difference" tones appear in such interactions and shows the relationship between the interaction tone frequency and its azimuthal mode number.

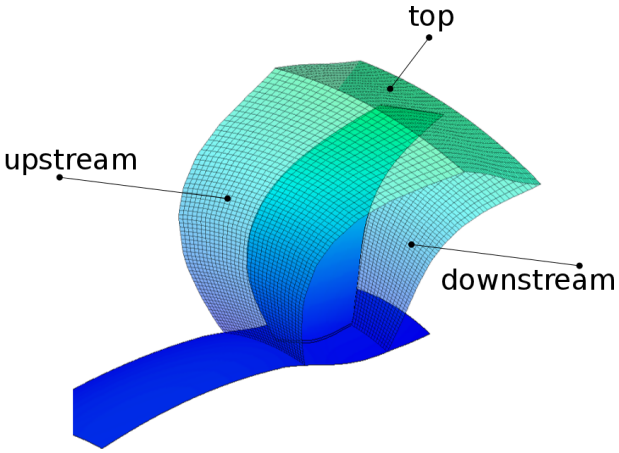

(a) Surfaces around one blade

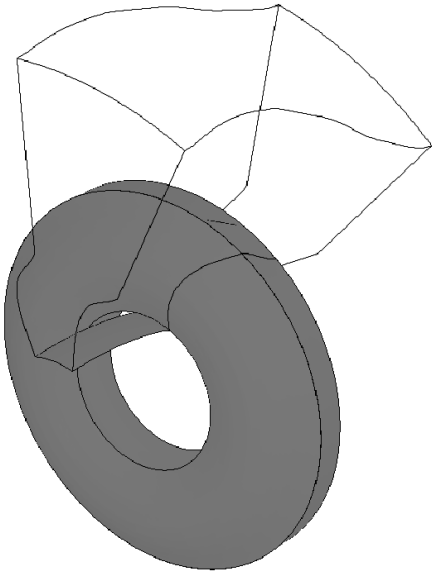

(b) Full-annulus FW-H surface

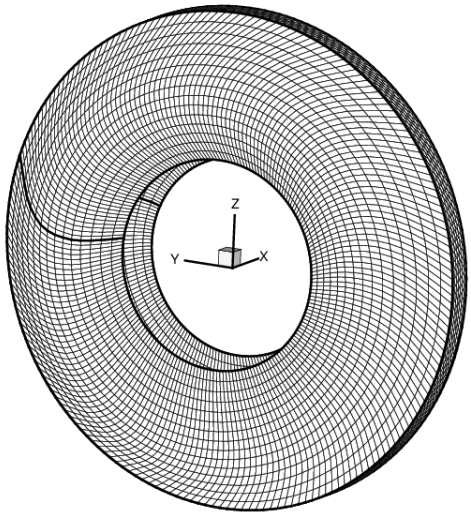

(c) Grid on FW-H surface

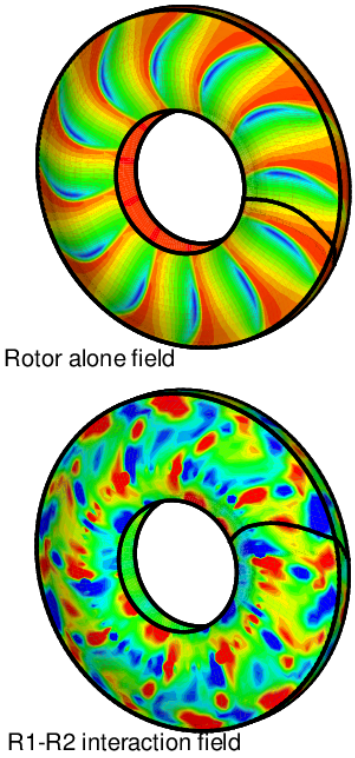

(d) Pressure contours

Figure 4. A description of the process of creating the FW-H surface: (a) surfaces in front (upstream), aft (downstream), and on top of (top) a single blade, (b) single passage to full annulus extension, (c) grid on the full FW-H surface, and (d) pressure contours on the FW-H surface for rotor alone and interaction noise computation. The two plots in (d) are on different scales.

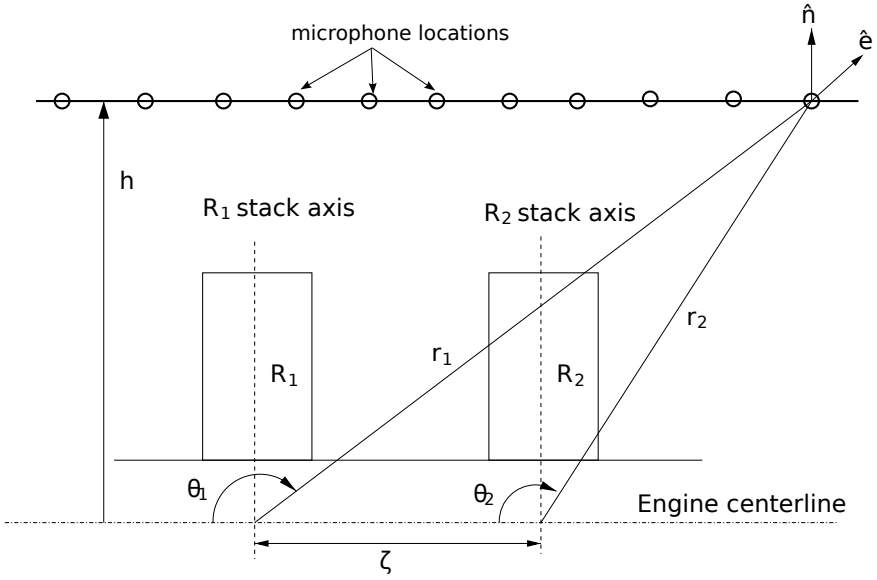

Figure 5. Schematic illustrating the sideline microphone locations.

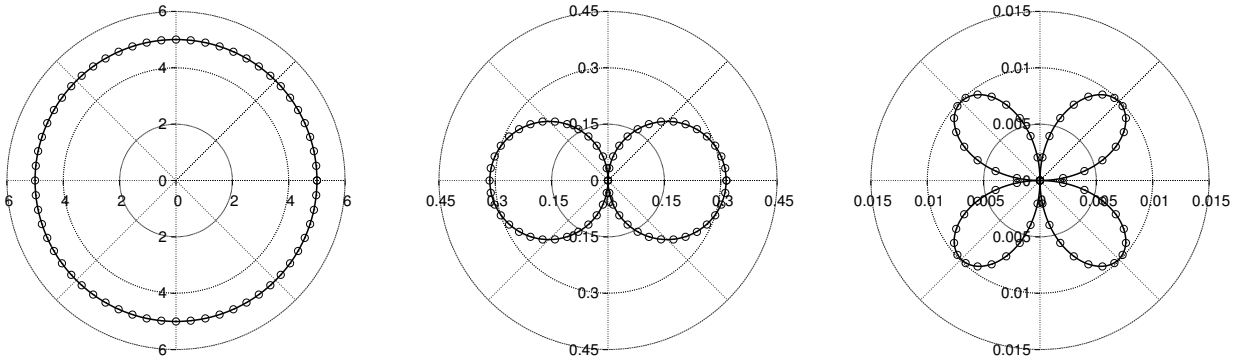

(a) Monopole (b) Dipole (c) Quadrupole

Figure 6. Directivity comparisons of pressure amplitude for a point source radiating in a quiescent medium between analytical solution (solid lines) and FW-H predictions (open circles). Pressure amplitudes are plotted in this polar plot.

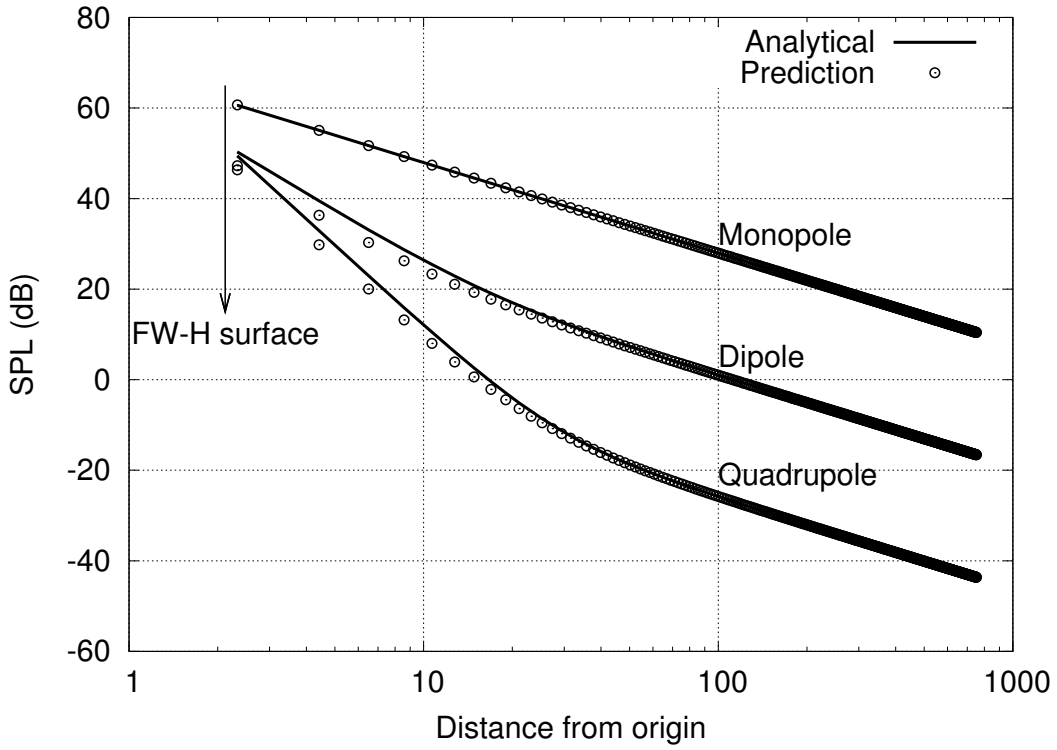

Figure 7. Near- and far-field comparisons of sound pressure levels (SPLs) between analytical solutions (solid lines) and FW-H predictions (open circles).

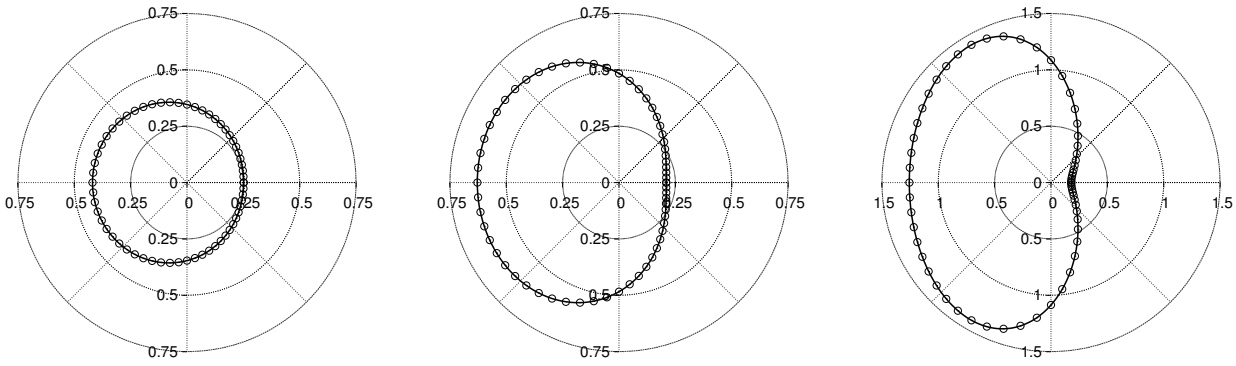

(a) M=0.25 (b) M=0.50 (c) M=0.75

Figure 8. Directivity comparisons of pressure amplitudes for a point source radiating in a moving medium between analytical solution (solid lines) and FW-H predictions (open circles). The axial flow Mach numbers considered are: (a) $M = 0.25$, (b) $M = 0.50$, and (c) $M = 0.75$.

Figure 9 compares the overall tone power level between prediction and data, which is obtained by adding (log sum) the acoustic power in the dominant tones. The frequency domain analyses is carried out for the first four harmonics of R1, which implies that the simulations only (theoretically) predict the following tones: $[1,(1\ldots\infty)],[2,(1\ldots\infty)],[3,(1\ldots\infty)]$ and $[4,(1\ldots\infty)]$. Since the geometric resolution (mesh) of the aft rotor is finite, only a finite number of "scattered" modes can be captured in the linearized runs. Only the first four scattered modes are therefore retained in the post-processing and used to compute the overall tonal power level. Similar filtering is applied to the experimental data as well to make a one-to-one comparison.

Figure 11 compares acoustic power in each tone between data and prediction. The agreement in general is good; the largest discrepancy is consistently observed for tones that should have a large azimuthal mode number if their source is rotor-rotor interaction. As an example, consider the $[3,1]$ tone. The frequency of this tone is $(3\times 12+1\times 10)\Omega = 46\Omega$ while its circumferential mode number is $(3\times 12-1\times 10)=26$. The radiation efficiency of this mode (would be given by $J_n(kr)$, $n=26$) is very low, due to the high order of the Bessel function. It is conjectured therefore that the origin of this tone is perhaps not simply R1-R2 interaction but perhaps interaction of a *spatially modulated* R1 wake with R2. Such a modulation occurring for example if the open rotor operates at a slightly non-zero angle of attack. The interaction of such spatially modulated wake would then produce the same time spectra content but the azimuthal order of the modes would be much lower, enhancing the radiation efficiency of these tones. This is seen consistently in the data, see e.g., tones $[4,1]$ and $[4,2]$ and the large difference between data and prediction for these tones.

Another evidence of "unsuspected" noise radiation in the open rotor experiment is observed (see Fig. 12) in the spectral decay of rotor alone tones, e.g., consider R1 alone tones: $[n,0]$, where $n=12,24,36,\ldots$ etc. Analytical theories e.g., due to Gutin[18] as well as the predictions made herein suggest a sharp dropoff with higher harmonics of noise due to thickness and steady loading, due again to rapid reduction in radiation efficiency (through increase in order of the Bessel function). Similar results (not shown here) were observed with other semi-analytical prediction methods.[19,20] Measured data shows some drop but it is not as much and also it plateaus out around the second blade passing frequency. Note that this level is still above the measured broadband noise. Again, it is suspected that measured noise here is perhaps due to a different source, e.g., inlet distortion. While there are turbulence screens employed in the experiment to minimize the inlet turbulence levels, there is still a possibility of having coherent turbulence structures chopped by the blades to produce tones at blade passing frequency. The azimuthal order of the pattern due to the interaction of these distortions with the rotor bladerows may be much lower than that for steady loading (thickness) noise source, making them highly efficient at radiating. It is suspected that noise due to such interaction masquerades as "rotor alone" tones especially at high frequencies.

Figure 10 shows the speed trend comparison for groups of tones. These are grouped based on the wake harmonic of the front rotor. For example, in the figure, $(1,\sum_1^4)$ refers to the sum of $[1,1],[1,2],[1,3]$ & $[1,4]$ tones. Analyzing the results in such groups is useful as it identifies the contribution of noise by a specific wake harmonic of the front rotor. Good agreement is observed for these sets of comparisons as well. It is also noted that the overall tone power level (in Fig. 9) is pretty much governed by the interaction of the first wake/vortex harmonic of R1 with R2 (i.e., by the $[1,\sum_1^4]$ tones). While this is true for the cases considered here, it may not always hold true (e.g., at other blade pitch and speed settings).

IV. Conclusion

A new prediction methodology utilizing linearized RANS analysis in combination with an integral method approach (Ffowcs Williams-Hawkings equation solution) is presented to predict aerodynamic noise from open rotors. A FW-H solver is developed and validated against analytical solutions of point sources (mono-, di-, and quadru-pole) in a quiescent medium as well as for a point monopole in a moving medium. The prediction process is then applied to the historic F31A31 baseline geometry recently tested at the NASA 9' x 15' low speed wind tunnel. Noise trends with blade tip Mach number are compared to show the validity of the prediction process. A very good agreement between prediction and data is observed in noise trends with blade tip speed. Absolute levels are slightly over-predicted (around 2-4 dB). Greatest mismatch between data and prediction (data being higher) is observed for tones which are expected to have very high circumferential mode number and therefore very low radiation efficiency. It is conjectured that the high acoustic power levels in such modes arise from "non-ideal" R1-R2 interaction such as may occur if the R1 wake was spatially modulated.

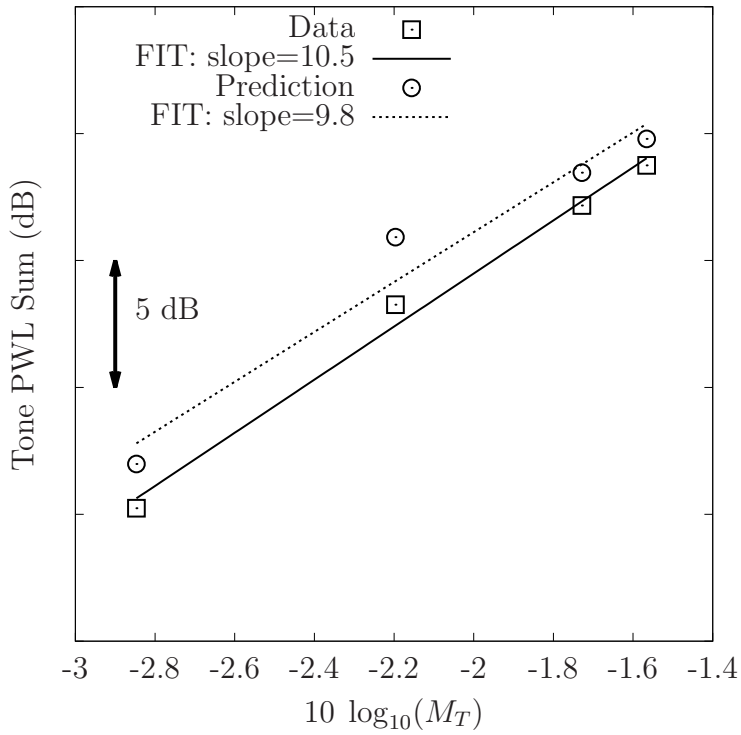

Figure 9. Comparison of measured and predicted sound power level sum of the rotor-rotor interaction tones.

V. Acknowledgment

The authors would like to thank their GE Aviation colleagues Dr. John Wojno and Dr. Muni Majjigi for providing critical technical guidance in the execution of this project, for providing the experimental data for validation, and for giving the permission to publish this work. Contributions from GE-GRC colleagues - Drs. Chingwei Shieh, Trevor Wood, Kishore Ramakrishnan, Lawrence Cheung, and Umesh Paliath in improving the prediction quality are also recognized. Thanks are also due to Dr. Ramani Mani who provided very valuable input on validation test cases.

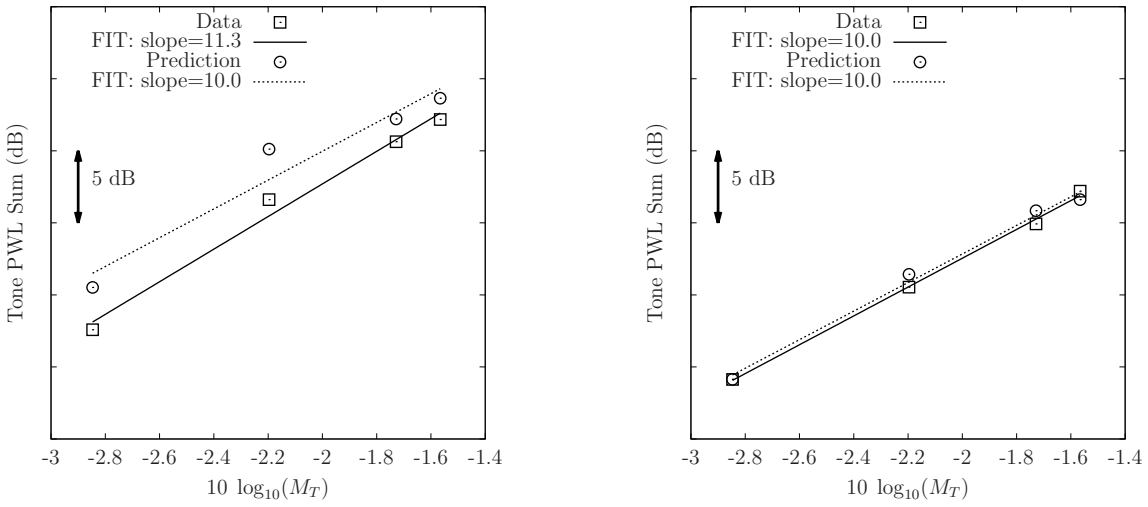

(a) $(1,\sum_1^4)$ tone sum

(b) $(2,\sum_1^4)$ tone sum

(c) $(3,\sum_1^4)$ tone sum

(d) $(4,\sum_1^4)$ tone sum

Figure 10. Comparison of measured and predicted sound power level sum grouped as blade passing harmonics of the front rotor.

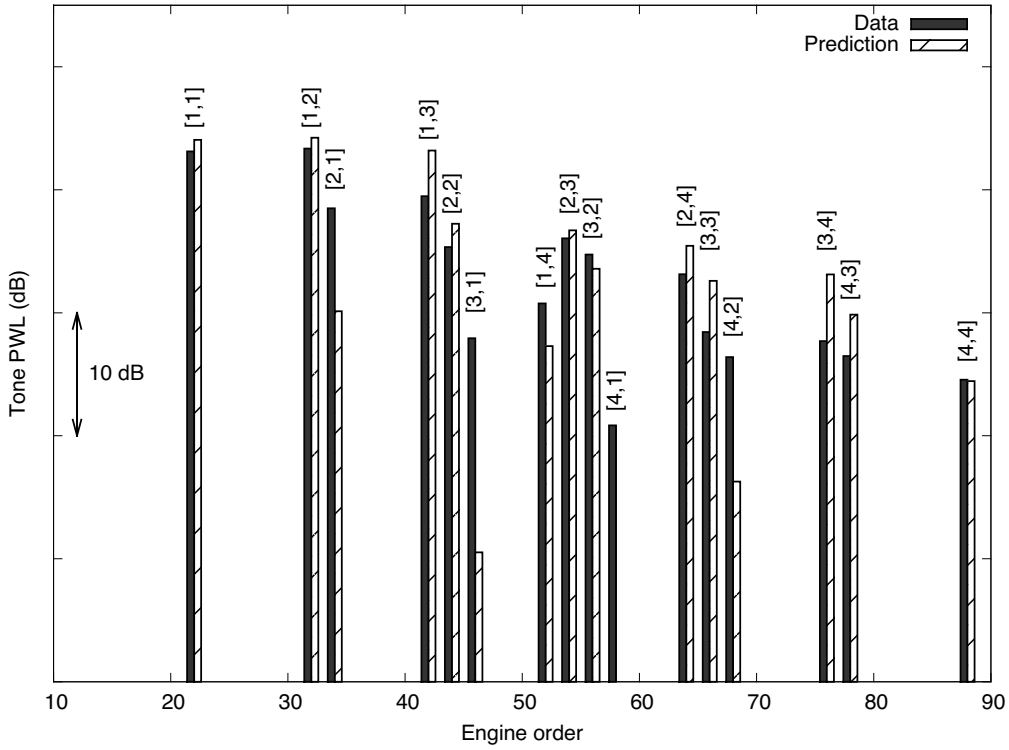

Figure 11. Interaction tone PWL spectra comparison between data and prediction at one sample operating point.

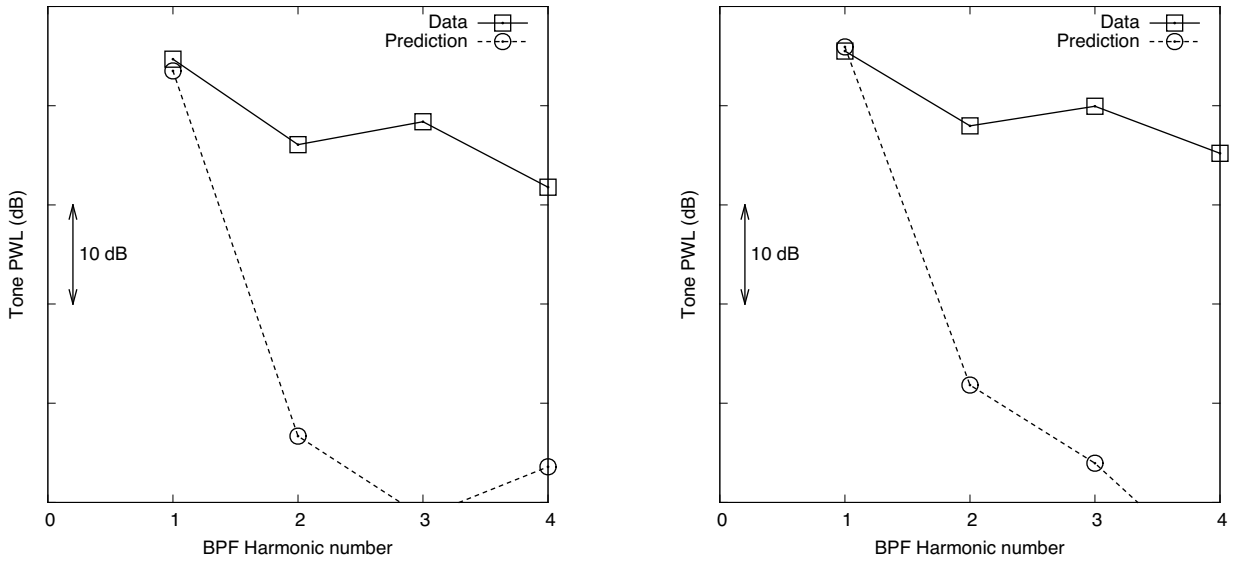

(a) R1 (b) R2

Figure 12. Variation of rotor alone acoustic power with (a) R1 and (b) R2 harmonics.

A. FW-H Formulation

The permeable surface Ffowcs Williams-Hawkings equation, upon ignoring the volume integral term, can be written as

$$4\pi\,|\mathbf{x}|\,p'(\mathbf{x},t) = \frac{x_i}{c\,|\mathbf{x}|}\frac{\partial}{\partial t}\int\left[p'n_i + \rho u_i(u_j - U_j)n_j\right]\,\mathrm{d}\Sigma + \frac{\partial}{\partial t}\int\left[\rho_0 u_i + \rho'(u_i - U_i)\right]n_i\,\mathrm{d}\Sigma. \tag{1}$$

The relation between source time, τ and observer time, t is

$$c(t-\tau) = |\mathbf{x} - \mathbf{x_s}| \tag{2}$$

Taking derivative of Eq. 2 w.r.t. τ yields

$$\begin{aligned}\frac{\mathrm{d}t}{\mathrm{d}\tau} - 1 &= \frac{\mathbf{x}-\mathbf{x_s}}{|\mathbf{x}-\mathbf{x_s}|}\cdot\frac{-\mathbf{U}}{c}\\ \frac{\mathrm{d}t}{\mathrm{d}\tau} &= 1 - M_r,\end{aligned} \tag{3}$$

which is the Doppler frequency shift. Also the relation between t and τ can be further expanded as

$$\begin{aligned}c(t-\tau) &= |\mathbf{x}-\mathbf{x_s}|\\ &\approx |\mathbf{x}| - \frac{\mathbf{x_s}.\mathbf{x}}{|\mathbf{x}|} \quad \text{for large } |\mathbf{x}|\,.\end{aligned}$$

Now, if the source $\mathbf{x_s}$ moves with velocity $\mathbf{U}$ then Eq. 4 can be further expanded

$$\begin{aligned}c(t-\tau) &\approx |\mathbf{x}| - \frac{\mathbf{x}.\mathbf{y}}{|\mathbf{x}|} - \frac{\tau\mathbf{U}.\mathbf{x}}{|\mathbf{x}|},\\ t-\tau &\approx \frac{|\mathbf{x}|}{c} - \frac{\mathbf{x}.\mathbf{y}}{c} - \frac{\tau\mathbf{U}.\mathbf{x}}{c},\\ (1-M_r)\tau &\approx t - \frac{|\mathbf{x}|}{c} + \frac{\mathbf{x}.\mathbf{y}}{c}.\end{aligned} \tag{4}$$

Take Fourier transform of Eq. 1.

$$\begin{aligned}4\pi\,|\mathbf{x}|\int_{-\infty}^{\infty} p'(\mathbf{x},t)e^{-\frac{i\omega t}{1-M_r}}\,\mathrm{d}t &= \frac{x_i}{c\,|\mathbf{x}|}\int_{-\infty}^{\infty}\left\{\frac{\partial}{\partial t}\int\left[p'n_i + \rho u_i(u_j-U_j)n_j\right]\,\mathrm{d}\Sigma\right\}e^{-\frac{i\omega t}{1-M_r}}\,\mathrm{d}t\\ &+ \int_{-\infty}^{\infty}\left\{\frac{\partial}{\partial t}\int\left[\rho_0 u_i + \rho'(u_i-U_i)\right]n_i\,\mathrm{d}\Sigma\right\}e^{-\frac{i\omega t}{1-M_r}}\,\mathrm{d}t.\end{aligned} \tag{5}$$

Convert $\frac{\partial}{\partial t} \to \frac{\partial}{\partial \tau}$ and $\mathrm{d}t \to \mathrm{d}\tau$ in above using Eq. 3 to get

$$\begin{aligned}4\pi\,|\mathbf{x}|\,\hat{p}(\mathbf{x},\frac{\omega}{1-M_r}) &= \frac{x_i}{c(1-M_r)\,|\mathbf{x}|}\int_{-\infty}^{\infty}\left\{\frac{\partial}{\partial \tau}\int\left[p'n_i + \rho u_i(u_j-U_j)n_j\right]\,\mathrm{d}\Sigma\right\}e^{-\frac{i\omega t}{1-M_r}}\,(1-M_r)\mathrm{d}\tau\\ &+ \frac{1}{(1-M_r)}\int_{-\infty}^{\infty}\left\{\frac{\partial}{\partial \tau}\int\left[\rho_0 u_i + \rho'(u_i-U_i)\right]n_i\,\mathrm{d}\Sigma\right\}e^{-\frac{i\omega t}{1-M_r}}\,(1-M_r)\mathrm{d}\tau.\end{aligned} \tag{6}$$

Using Eq. 4 to rewrite t in terms of τ we get

$$\begin{aligned}4\pi\,|\mathbf{x}|\,\hat{p}(\mathbf{x},\frac{\omega}{1-M_r}) &= \frac{x_i}{c\,|\mathbf{x}|}\int_{-\infty}^{\infty}\left\{\frac{\partial}{\partial \tau}\int\left[p'n_i + \rho u_i(u_j-U_j)n_j\right]\,\mathrm{d}\Sigma\right\}e^{-i\omega\tau}\mathrm{d}\tau e^{-\frac{i\omega}{1-M_r}\left(\frac{|\mathbf{x}|}{c}-\frac{\mathbf{x}.\mathbf{y}}{c|\mathbf{x}|}\right)}\\ &+ \int_{-\infty}^{\infty}\left\{\frac{\partial}{\partial \tau}\int\left[\rho_0 u_i + \rho'(u_i-U_i)\right]n_i\,\mathrm{d}\Sigma\right\}e^{-i\omega\tau}\,\mathrm{d}\tau\,e^{-\frac{i\omega}{1-M_r}\left(\frac{|\mathbf{x}|}{c}-\frac{\mathbf{x}.\mathbf{y}}{c|\mathbf{x}|}\right)}.\end{aligned} \tag{7}$$

Dropping the constant phase shift term $\exp\left(-\frac{i\omega}{1-M_r}\frac{|\mathbf{x}|}{c}\right)$ from above, the following is obtained

$$\begin{aligned}4\pi\,|\mathbf{x}|\,\hat{p}(\mathbf{x},\frac{\omega}{1-M_r}) &= \frac{x_i}{c\,|\mathbf{x}|}\int_{-\infty}^{\infty}\left\{\frac{\partial}{\partial \tau}\int\left[p'n_i + \rho u_i(u_j-U_j)n_j\right]\,\mathrm{d}\Sigma\right\}e^{-i\omega\tau}\mathrm{d}\tau e^{-\frac{i\omega}{1-M_r}\left(-\frac{\mathbf{x}.\mathbf{y}}{c|\mathbf{x}|}\right)}\\ &+ \int_{-\infty}^{\infty}\left\{\frac{\partial}{\partial \tau}\int\left[\rho_0 u_i + \rho'(u_i-U_i)\right]n_i\,\mathrm{d}\Sigma\right\}e^{-i\omega\tau}\,\mathrm{d}\tau\,e^{-\frac{i\omega}{1-M_r}\left(-\frac{\mathbf{x}.\mathbf{y}}{c|\mathbf{x}|}\right)}.\end{aligned} \tag{8}$$

Now $\partial/\partial\tau$ can be taken inside the Σ integral as it is independent of τ. Also, the following property,

$$\int_{-\infty}^{\infty} \frac{\partial\psi(t)}{\partial t} \exp\left(-i\omega t\right)\mathrm{d}t = i\,\omega \int_{-\infty}^{\infty} \psi(t) \exp\left(-i\omega t\right)\mathrm{d}t, \tag{9}$$

can be used to rewrite Eq. 8 as

$$\begin{aligned} 4\pi\,|\mathbf{x}|\,\hat{p}(\mathbf{x}, \frac{\omega}{1-M_r}) &= \frac{x_i}{c\,|\mathbf{x}|} \int \left[p' n_i + \rho \widehat{u_i(u_j} - U_j) n_j\right] \exp\left\{-\frac{i\omega}{1-M_r}\left(-\frac{\mathbf{x}.\mathbf{y}}{c\,|\mathbf{x}|}\right)\right\} \mathrm{d}\Sigma \\ &+ \int \left[(\rho_0 u_i + \widehat{\rho'(u_i} - U_i)) n_i\right] \exp\left\{-\frac{i\omega}{1-M_r}\left(-\frac{\mathbf{x}.\mathbf{y}}{c\,|\mathbf{x}|}\right)\right\} \mathrm{d}\Sigma. \end{aligned} \tag{10}$$

APPENDICES

B. R1-R2 Interaction Noise

A mathematical reasoning for the generation of sum and difference tones in R1-R2 interaction is given below. In stationary frame (x, r, θ, t), R1 wake can be represented by

$$V_g = \sum_{n=0}^{\infty} \hat{V}_g \exp\left\{i\ n\ N_{R_1}(-\Omega_1 t + \theta)\right\}, \tag{11}$$

where Ω_1 is the angular velocity of rotor 1. In the frame of reference attached to the aft rotor (x', r', θ', t') where

$$x' = x, r' = r, t' = t, \&\theta' = \theta + \Omega_2 t$$

the gust is

$$V_g = \sum_{n=0}^{\infty} \hat{V}_g \exp\left\{i\ n\ N_{R_1}(-(\Omega_1 + \Omega_2)t + \theta'))\right\}. \tag{12}$$

Hence, the frequency of the gust in rotor 2 frame of reference appears as $\omega_g' = nN_{R_1}(\Omega_1 + \Omega_2)$. This is the frequency used at which the linearized RANS, forced response calculation is carried out in R2. The solution of the linearized RANS equations yields near-field pressure in R2 frame of reference, which may be written as

$$p = \sum_{n=0}^{\infty} \sum_{k=-\infty}^{\infty} \hat{p} \exp\left\{i(-\omega t + m'\theta')\right\}, \tag{13}$$

where $m' = nN_{R_1} - kN_{R_2}$ as given by the Tyler-Sofrin theory. Writing the above expression in the ground frame of reference gives

$$\begin{aligned} p &= \sum_{n=0}^{\infty} \sum_{k=-\infty}^{\infty} \hat{p} \exp\left\{i(-nN_{R_1}(\Omega_1 + \Omega_2)t + (nN_{R_1} - kN_{R_2})(\theta + \Omega_2 t))\right\} \\ &= \sum_{n=0}^{\infty} \sum_{k=-\infty}^{\infty} \hat{p} \exp\left\{i(-(nN_{R1}\Omega_1 + kN_{R_2}\Omega_2)t + (nN_{R_1} - kN_{R_2})\theta)\right\} \\ &, \end{aligned} \tag{14}$$

Equation 14 suggests that the frequencies of the R1-R2 interaction tones, and the corresponding circumferential modes are given by

$$\omega_p = (nN_{R_1}\Omega_1 + kN_{R_2}\Omega_2); \quad m = nN_{R_1} - kN_{R_2}.$$

Note that Ω_1 and Ω_2 are magnitudes of the rotation rates; the direction of rotation is taken into account in relating θ' to θ. For the case when the shaft rotation rate for both rotors is the same ($\Omega_1 = \Omega_2 = \Omega$), the expression for interaction frequencies reduces to

$$\omega_p = (nN_{R_1} + kN_{R_2})\Omega, \quad \text{where } -\infty < k < \infty,$$

and hence the expression "sum" and "difference" tones is used to refer to rotor-rotor interaction tones.

Note that while the "sum" tones are easily observed in experiments, the "difference" tones are difficult to observe. This is primarily because the circumferential mode number corresponding to a "difference" tone is much higher (which corresponds to the order of the Bessel function) while the frequency (which corresponds to the argument of the Bessel function) is much lower, thus rendering the radiation efficiency of "difference" tones to be very low.

References

[1]A. B. Parry, M. Kingan, and B. J. Tester, "Relative Importance of Open Rotor Tone and Broadband Sources," *Proceedings of the 17th AIAA/CEAS Aeroacoustics Conference (32nd AIAA Aeroacoustics Conference)*, Portland, OR, 2011.

[2]A. Sharma, S. K. Richards, T. H. Wood, and C. M. Shieh, "Numerical Prediction of Exhaust Fan-Tone Noise from High-Bypass Aircraft Engine," *AIAA Journal*, Vol. 47, No. 12, 2009.

[3]J. Verdon, "Linearized Unsteady Aerodynamic Analysis of the Acoustic Response of Wake/Blade-Row Interaction," *NASA/CR–2001-210713*, 2001.

[4]D. Prasad and J. M. Verdon, "A Three-Dimensional Linearized Euler Analysis of Classical Wake/Stator Interactions: Validation and Unsteady Response Predictions," *International Journal of Aeroacoustics*, Vol. 1, No. 2, 2002, pp. 137–163.

[5]J. E. Ffowcs Williams and D. L. Hawkings, "Sound Generated by Turbulence and Surfaces in Arbitrary Motion," *Philosophical Transactions of the Royal Society*, Vol. A264, No. 1151, 1969, pp. 321–342.

[6]D. G. Holmes, B. E. Mitchell, and C. B. Lorence, "Three Dimensional Linearized Navier-Stokes Calculations for Flutter and Forced Response," *Proceedings of the 8th ISUAAT Symposium*, Stockholm, Sweden, 1997.

[7]M. Nyukhtikov, N. Smelova, B. E. Mitchell, and D. G. Holmes, "Optimized Dual-Time Stepping Technique for Time-Accurate Navier-Stokes Calculations," *Proceedings of the 14th ISUAAT Symposium*, Duke University, 2003.

[8]Hubbard, H. H., "Sound from Dual-Rotating and Multiple Rotating Propellers," Tech. rep., NACA TN 1654, 1948.

[9]Hanson, D. B., "Noise of Counter-rotation Propellers," *AIAA Journal of Aircraft*, Vol. 22, No. 7, 1985, pp. 609–617.

[10]D. B. Hanson, "Compressible Helicoidal Surface Theory for Propeller Aerodynamics and Noise," *AIAA Journal*, Vol. 21, No. 6, 1983, pp. 881–889.

[11]Mani, R., "The Radiation of Sound from a Propeller at Angle of Attack," *Proceedings of the Royal Society A*, Vol. 431, No. 1882, 1990, pp. 203–218.

[12]D. B. Hanson, "Sound from a Propeller at Angle of Attack: A New Theoretical Viewpoint," *Proceedings of the Royal Society A*, Vol. 449, No. 1936, 1995, pp. 315–328.

[13]A. Carazo, M. Roger, and M. Omais, "Analytical Prediction of Wake-Interaction Noise in Counter-Rotation Open Rotors," *17th AIAA/CEAS Aeroacoustics Conference, AIAA 2011-2758*, June 2011.

[14]V. P. Blandeau and P. F. Joseph, "Broadband noise due to rotor-wake/rotor interaction in contra-rotating open rotors," *AIAA Journal*, Vol. 11, No. 48, 2010, pp. 2674–2686.

[15]A. Peters and Z. S. Spakovszky, "Rotor Interaction Noise in Counter-Rotating Propfan Propulsion Systems," *Journal of Turbomachinery*, Vol. 134, No. 1, 2012.

[16]D. B. Stephens and E. Envia, "Acoustic Shielding for a Model Scale Counter-Rotation Open Rotor," *Proceedings of the 17th AIAA/CEAS Aeroacoustics Conference*, Portland, Oregon, 2011.

[17]A. Sharma, H. Chen, and C. M. Shieh, "Linearized Navier-Stokes Analysis for Rotor-Stator Interaction Tone Noise Prediction," *16th AIAA Aeroacoustics Conference, Paper 2010-3744*, Stockholm, Sweden, 2010.

[18]Gutin, L., "On the Sound Field of a Rotating Propeller," Tech. rep., NACA TM 1195, 1948.

[19]C. E. Whitfield and P. R. Gliebe, "Predicted Vs. Scale Model and Flight Test UDFR Engine Noise," *13th AIAA Aeroacoustics Conference, Paper 90-3936*, Tallahassee, Florida, USA, 1990.

[20]C. E. Whitfield, R. Mani, and P. R. Gliebe, "High Speed Turboprop Aeroacoustic Study," *NASA Contractor Report 185241*, 1990.